Journal of Statistical Physics, Vol. 120, Nos. 5/6, September 2005 (© 2005)
DOI: 10.1007/s10955-005-6989-y

Random Tilings of High Symmetry: I. Mean-Field Theory

N. Destainville,[1] M. Widom,[2] R. Mosseri,[3] and F. Bailly[4]

Received December 11, 2004; accepted April 29, 2005

We study random tiling models in the limit of high rotational symmetry. In this limit a mean-field theory yields reasonable predictions for the configurational entropy of free boundary rhombus tilings in two dimensions. We base our mean-field theory on an iterative tiling construction inspired by the work of de Bruijn. In addition to the entropy, we consider correlation functions, phason elasticity and the thermodynamic limit. Tilings of dimension other than two are considered briefly.

KEY WORDS: Random tiling; mean field theory; quasicrystal; entropy.

1. INTRODUCTION

The discovery of quasicrystals by Shechtman *et al.*,[1] and the proposal of Levine and Steinhardt[2] of their possible relationship with Penrose tilings,[3] motivated widespread investigation of tilings as models for quasicrystal structure. It is presumed that energetically favored atomic motifs form geometrical tiles, and that these tiles may be arranged quasiperiodically in space to describe the quasicrystal structure. We consider tiling models defined as projections from a higher D-dimensional lattice into a lower d-dimensional physical space. For example, 10-fold symmetric tilings may be projected from $D = 5$ into $d = 2$, and icosahedral tilings may be

[1]Laboratoire de Physique Théorique, UMR CNRS-UPS 5152, Université Paul Sabatier, 31062 Toulouse Cedex 04, France.
[2]Department of Physics, Carnegie Mellon University, Pittsburgh, PA 15213, USA; e-mail: widom@andrew.cmu.edu
[3]Laboratoire de Physique Théorique des Liquides, Tour 24, Boîte 121, 4, Place Jussieu, 75252 Paris Cedex 05, France.
[4]LPSB-CNRS, 92195 Meudon Cedex, France.

projected from $D=6$ into $d=3$. Figure 1 displays examples of tilings constructed as projections from D-dimensional simple cubic lattices into $d=2$-dimensional physical space. The difference between the higher dimension D and the tiling dimension d is called the *codimension*.

An important unsolved problem is understanding the interactions among tiles that may favor particular tile arrangements over others. The suggestion by Elser[4] that random tilings spontaneously exhibit quasiperiodicity, created a subfield within the area of tiling theory.[5] It was shown,[6] for at least one atomistic model quasicrystal,[6,7] that quasicrystalline order emerges with random tiling, rather than Penrose-like, order. The best description for real quasicrystalline materials remains an open problem, depending whether one assumes that energetic interactions favor quasiperiodicity[8] or that entropy stabilizes the quasicrystal structure at high temperatures.[5,6,9]

In addition to their role in the theory of quasicrystals, random tiling models appear in a number of other interesting scientific contexts. Their combinatorial properties, for example their relationship to generalized partitions[10–12] make them interesting models for study within pure mathematics.[13–20] Some random tiling models provide examples of exactly solvable models[21–23] of interest within statistical mechanics. We note a relationship with algorithms for sorting lists.[24,25] Random tiling models have also been proposed as models for elastic membranes.[11,26]

The random tiling theory of quasicrystals focuses on two important properties: The tiling entropy contributes to the configurational entropy of the quasicrystal, reducing its free energy and enhancing thermodynamic stability against other competing phases,[9] Variation of the entropy with average phason strain defines the phason elastic constants. Table I summarizes existing data on the configurational entropies of $d=2$ rhombus tilings, showing a trend of monotonic increase with D. Table II shows corresponding data for $d=3$ rhombohedron tilings.

Techniques employed in theoretical studies include analytic exact solution,[22,23] Monte Carlo computer simulation[27] and numerical transfer

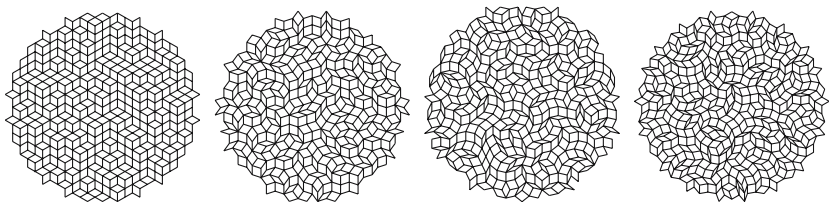

Fig. 1. Examples of free boundary $d=2$ tilings with $D=3, 5, 7$ and 9.

Table I. $d=2$ strain-free rhombus tiling entropies

D	2	3	4	5	∞
σ	0	0.323	0.434	0.481	0.568

Table II. $d=3$ strain-free rhombohedron tiling entropies

D	3	4	5	6	∞
σ	0	0.214	NA	0.24	<0.323

matrix methods.[28] While these methods prove successful at calculating quantitative values for entropy and elastic constants, they are not always easy to implement, and they often do not enhance our intuitive and qualitative understanding of the problem. The technique of mean-field theory[29] in statistical mechanics provides an approximation that can be analytically simple to implement and can provide a direct link between quantitative calculation and our qualitative picture of the physics of the problem. Mean-field theory often becomes exact in certain limits, such as the limit of infinite dimension. A mean-field theory for random tilings has never been precisely defined.

The search for an analogue of mean-field theory applicable to random tilings motivates our study of random tiling models with high rotational symmetry. We anticipate[5] that the infinite D limit may prove easier to analyze than specific finite values of D. Experience gained in the study of this limit may later be transfered back to the finite D values of greatest physical interest. Furthermore, a study of D dependence of entropy or elastic constants might in itself yield qualitative understanding of the values of entropy and elastic constants for small D. Other researchers[30–32] have studied deterministic quasiperiodic tilings of arbitrary rotational symmetry, but have considered neither the high symmetry limit nor the case of random tilings.

We mention, in addition, that high symmetry tilings are good candidates of models for topologically disordered graphs, different from the usual random graphs[33] because the coordination number of a vertex is a random variable, with algebraically decreasing long-range correlations. Quantum diffusion on such tilings has recently been studied by Vidal *et al.*, and was found to exhibit an interesting diffusive behavior.[34] These tilings could even prove interesting as models for structural glasses.

A word of caution should be given on the title referring to "high symmetry" tilings. In two dimensions, this statement is unambiguous owing to the possibility of generating tilings whose Fourier spectrum will display point symmetries of arbitrary order. In three dimensions however, the highest point group symmetry, the icosahedral one of order 120, is already reached with codimension three tilings. "High symmetry", in three and higher dimensions, has therefore a less formal meaning in our description. For a given tiling in dimension d, we can map the whole set of edge orientations onto points on a $(d-1)$-dimensional hypersphere. As D increases, these representative points cover more and more densely the hypersphere, approaching, but never meeting, the highest continuous point symmetry of the hypersphere itself. This is what is meant by "high symmetry" in the title.

Two previous papers[25,35] presented initial studies of this problem. The first paper proposed an upper bound on the entropy in the limit of large D and discussed problems associated with the thermodynamic limit of tiling models. The second one[35] presented a preliminary mean-field approach of the entropy calculation. In the present paper, we explain the previous work in greater detail. In addition, we inspect spatial correlations and phason elasticity. All tilings considered in this paper are free boundary tilings (see Section 2). Fixed boundary tilings are analyzed by computer simulation in the following paper.[36] Table III summarizes the available estimates of the large D entropy.

The organization of this paper is as follows: We begin in Section 2 with definitions and concepts that apply generally to random tiling models. Then, in Section 3 we describe our mean-field theory of two-dimensional tilings of high rotational symmetry. We start with an upper bound (Section 3.1) then a more accurate estimate (Section 3.2) based on path counting arguments. We investigate the nature of spatial correlations in Section 3.3 followed by consideration on finite D corrections.

Table III. Entropy estimates in the large *D* limit

Value	Method	Reference
0.998	Rigorous upper bound	24
0.693	Conjectured upper bound upper bound	Eq. (30)
0.6	Extrapolated exact values	Ref. 25
0.598	Mean-field theory	Eq. (37)
0.568	Monte Carlo simulation	Ref. 30
0.231	Rigorous lower bound	24

Section 4 tackles de Bruijn line interactions and phason elasticity. Tilings of dimension $d \neq 2$ are examined in Section 5.

2. CHARACTERIZATION OF TILINGS

In this section, we introduce the basic material used throughout the paper to characterize and manipulate two-dimensional random tilings.

A tiling is a covering, without gaps or overlaps, of a given region of a d-dimensional Euclidean space. In the present paper, the tiles are d-dimensional rhombohedra, which we will generically call "rhombi" in the following.

Tiling systems can have different boundary conditions, such as free, fixed or periodic ones. For example, the tilings in Fig. 1 illustrate free boundary tilings of various rotational symmetries. The free boundary thermodynamic limit is taken as follows: Consider all tilings that cover a circular region of space $\mathcal{R}$ (whose area will tend towards infinity). For a given $\mathcal{R}$, tilings contain fixed numbers of tiles of each type, with relative frequencies governed by the average composition of the tiling we wish to study. The total number of tiles is chosen so they encompass a total area slightly larger than area of the region $\mathcal{R}$ that must be covered. Every tile must intersect $\mathcal{R}$ or share an edge with a tile that does so. This ensures a reasonably compact tiling and gives us needed control over the composition.

It is generally supposed that free and periodic boundary tilings have the same entropies (provided their compositions match) at the thermodynamic limit. But fixed boundary tilings display a less usual behavior: such boundaries have such a macroscopic effect on tilings that their entropy per tile at the infinite size limit can be strictly smaller than the free boundary one. For example, in the case of "hexagonal" tilings of 60° rhombi ($D=3$ and $d=2$), when all orientations of rhombi occur with equal probability, the fixed boundary entropy per tile $\sigma_{\text{fixed}} = 0.261$[37] while the free boundary entropy per tile $\sigma_{\text{free}} = 0.323$.[38] In addition to a qualitative argument by Elser,[37] this phenomenon has more recently been rigorously explained and described[39,17,18] the local entropy density can be calculated in any point of the tiling; it displays a gradient between the regions near the boundary, where the entropy is vanishing, and the central region, where the entropy is a free boundary one. In other words, it is only at the very center of the tiling that the tiling loses the influence of the boundary.

2.1. Membrane Representation of Tilings

Here, we briefly recall how tilings are conveniently coded by (mono-valued) functions from the "physical real space" to the "perpendicular" space.

Rhombic tiles can be considered as the projections onto a d-dimensional space of the d-dimensional faces of a hypercube in a space of higher dimension D. Conversely, any rhombic tiling in the d-dimensional space can be "lifted" to a d-dimensional continuous membrane embedded in the $\mathbf{Z}^D$ hypercubic lattice. When this membrane is projected back into d-dimensional space, the facets of the D-dimensional lattice project precisely onto the d-dimensional rhombic tiles. Such a membrane is said to be *continuous* and *directed* to emphasize the fact that, when projected, is does not exhibit any gaps or overlaps. We say that we are dealing with $D \to d$ membranes or tilings. This *membrane* representation of rhombus tilings[5,11,26,39] is a useful tool in quasicrystal science.

Notation related to the D-dimensional geometry and projection is described in appendix 6. Let $(\hat{\mathbf{e}}_i)_{i=1,\dots,D}$ denote the basis of the $\mathbf{Z}^D$ hypercubic lattice and denote by $\hat{\mathbf{e}}_i^{\parallel}$ the normalized projection of $\hat{\mathbf{e}}_i$ on the d-dimensional space where tilings lie. The projection direction is (arbitrarily) chosen so that the basis vectors $\hat{\mathbf{e}}_i^{\parallel}$ all have equal length and angles that are multiples of π/D (see appendix A). We call this collection of vectors a *regular fan*.

A rhombic tile has d edge orientations $\{\hat{\mathbf{e}}_i^{\parallel}, \hat{\mathbf{e}}_j^{\parallel}, \dots, \hat{\mathbf{e}}_k^{\parallel}\}$ with $(1 \leqslant i < j < \cdots < k \leqslant D)$. We denote this tile species as $T_{ij\cdots k}$. Note that there are $\binom{D}{d}$ different species of tiles. Examples of $D \to 2$ tilings are displayed in Fig. 1. The first one can be seen as a membrane embedded in a 3-dimensional cubic lattice, as may be more clear in the following Fig. 2.

Such random tilings have internal degrees of freedom, the so-called *localized phason flips*, which consist of local rearrangements of tiles. Such local flips are displayed in Fig. 3. In d dimensions, a flip involves $d+1$ tiles that fill a small zonotope.[40] Note that in 2 dimensions, the ergodicity of tiling ensembles *via* elementary flips is proven,[12,14] whereas it is an

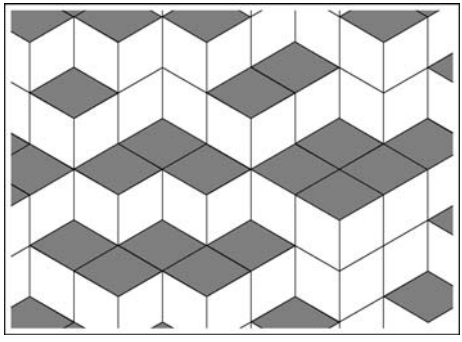

Fig. 2. Three-dimensional image effect. Gray rhombi can be seen as horizontal terraces.

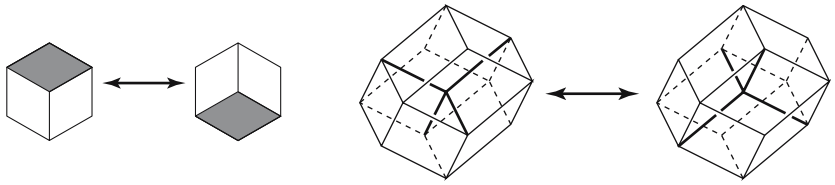

Fig. 3. Two examples of elementary flips in 2 and 3 dimensions, involving respectively 3 and 4 rhombic tiles.

open question in three and more dimensions, even if some significant progress has been achieved recently.[41] This local degree of freedom is the source of configurational entropy in random tilings.

A functional representation of these directed membranes will prove useful. Denote the d-dimensional "physical" or "real" space containing the actual tiles by $\mathcal{E}^{\parallel} = \boldsymbol{R}^d$, and the perpendicular $(D-d)$-dimensional space by $\mathcal{E}^{\perp} = \boldsymbol{R}^{D-d}$. Since membranes representing tilings are directed, they are the graphs of single-valued continuous functions $h: \mathcal{E}^{\parallel} \to \mathcal{E}^{\perp}$. Such functions h are called the *height functions* of the corresponding tilings. The detailed construction of the spaces $\mathcal{E}^{\parallel}$ and $\mathcal{E}^{\perp}$ is described in appendix A when $d=2$. Executing an elementary flip of vertex v changes the value of the height function locally at vertex v.

Since the membranes are embedded in a hypercubic lattice, they are irregular and faceted at on the length scale of individual tiles. The local height function h is usually coarse-grained to get a smoother function $\bar{h}$ which closely tracks the local function h over long distances but which is nearly insensitive to individual single vertex flips.[5,11,42] The function $\bar{h}$ describes a smoothed membrane. Then one defines the *phason gradient* $\boldsymbol{E} = \nabla \bar{h}$. This $(D-d) \times d$-dimensional tensor controls the fractions of the different species of tiles.

The entropy can be written as a functional of the phason gradient.[5] Moreover, the random tiling model hypothesis states that this latter entropy has a unique maximum, corresponding to tile fractions maximizing the symmetry. The orientation of the real space $\mathcal{E}$ is chosen so that the gradient is zero at this maximum, and the model states that the entropy density has a quadratic behavior near this maximum:

$$\sigma = \sigma_{\max} - \frac{1}{2} \nabla \bar{h} \cdot \mathbf{K} \cdot \nabla \bar{h} + o(|\nabla \bar{h}|^2). \tag{1}$$

By analogy with an usual elastic theory, the tensor $\mathbf{K}$ is called the tensor of *phason elastic constants*.

The best known rhombus tilings of the plane is the Penrose[3] tiling, which displays an exact quasiperiodicity. The membrane representation of a Penrose tiling is a flat, horizontal, sheet. The phason strain of this tiling vanishes. In addition, the Penrose tiling is virtually unique (up to translations) because it forbids localized phason flips. The random tiling hypothesis implies that the most typical tilings in a random tiling ensemble mimic the long-range order of the Penrose tiling, while enjoying the entropy of short-range fluctuations.

Random and perfect tilings with vanishing phason strain exhibit the highest symmetry consistent with the projection from $D \to d$. In two dimensions, this symmetry includes[32] $2D$-fold rotational symmetry. A given tiling itself generally has no point about which it is invariant under rotations, but two-point and higher correlation functions do exhibit the symmetry. In addition, there are two families of mirror symmetries, denoted "along" and "between" according to the relation between the mirror plane and the basis vectors $\hat{\mathbf{e}}_i^{\parallel}$.

2.2. De Bruijn Dualization and Iterative Construction of Tilings

The de Bruijn dualization[43] provides another representation of random tilings. We present this technique in two dimensions and generalize it to higher dimensions when needed.

De Bruijn grids[43–45] are made up of lines, the de Bruijn lines, that are sometimes called *worms*. These lines are made of adjacent tiles sharing an edge of given orientation. It is always possible to extend these lines through the whole tiling up to a boundary tile. An example is presented in Fig. 4. Since there are D different edge orientations, there are D different de Bruijn families. A rhombic tile corresponds to the intersection of two lines of different families. Hence there are $\binom{D}{2} = D(D-1)/2$ tile species. There are no triple intersections, and lines of a same family never intersect, even in an infinite tiling, because no rhombus has four parallel edges.

This de Bruijn representation of tilings suggests an iterative construction of $D \to 2$ tilings in terms of directed random walkers on $D-1 \to 2$ tilings. The basic idea is illustrated in Fig. 4. A $D-1 \to 2$ tiling is sheared to make room for a new de Bruijn line family by taking the vectors $\hat{\mathbf{e}}_i^{\parallel}$ that initially lie at angles $\pi i/(D-1)$ and replacing them with angles $\pi i/D$ (see Fig. 4, left). Next, paths are chosen on the $D-1 \to 2$ tiling (dark lines in Fig. 4, left). They go from bottom to top, as symbolized by a "time arrow" t. These paths must be "opened" in the direction $\hat{\mathbf{e}}_D^{\parallel}$ in order to form de Bruijn lines (shaded in Fig. 4 right) of the Dth family and therefore a $D \to 2$ tiling. These paths are directed in the positive time direction

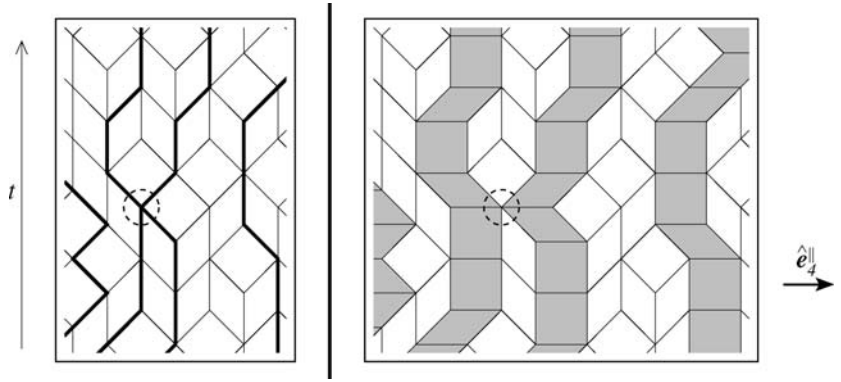

Fig. 4. Iterative process for the construction of $D \to 2$ tilings. Left shows paths on a re-oriented $3 \to 2$ tiling. Right shows the resulting $4 \to 2$ tiling. A non-crossing contact between two de Bruijn lines of the same family is emphasized.

and they do not intersect within the same family. The figure shows a contact among paths that is not an intersection. Conversely, de Bruijn lines of family D in a $D \to 2$ tiling may be collapsed to directed walks in a $D-1 \to 2$ tiling. There is thus a one-to-one correspondence between $D \to 2$ tilings with p de Bruijn lines of family D and collections of p non-intersecting walks on $D-1 \to 2$ tilings.

2.3. Grid Parameters, Phason Strain and Tile Fractions

In this section, we introduce several macroscopic quantities that characterize a two-dimensional random tiling. Apart from the phason gradient $\boldsymbol{E}$ previously defined, a tiling can also be characterized at large scale either by the tile fractions or by geometric parameters. This section also provides the relationships between these quantities (2.3.2) as well as useful relations that constrain them (2.3.3).

2.3.1. Definitions

We now address two macroscopic characterizations of de Bruijn lines, the mean line spacings and orientations, and link these to the phason strain $\mathbf{E}$ and the tile fractions n_{ij} (the fraction of tiles that are of type T_{ij}). De Bruijn lines of family i are characterized by the mean spacing l_i between two lines of the family i and the mean angle ϕ_i that lines of this family make with their nominal direction. The nominal direction (denoted by $\boldsymbol{\delta}_i$) is normal to $\hat{\mathbf{e}}_i^{\parallel}$ (see Fig. 5). For a maximally symmetric tiling with vanishing phason strain $\mathbf{E} = 0$, rotational symmetry guarantees that the

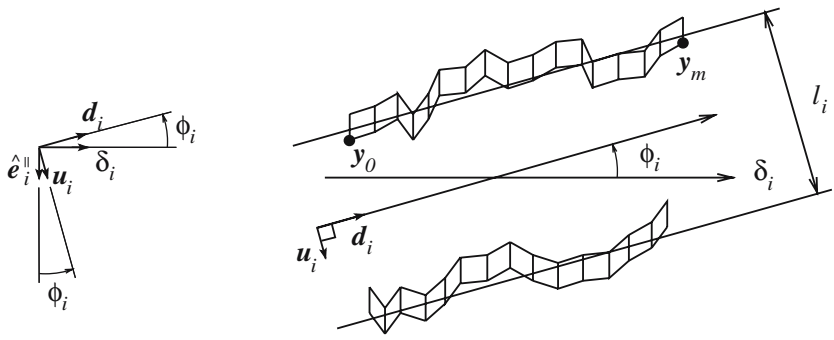

Fig. 5. Definition of quantities l_i – the mean distance between two neighbor lines of the i-th de Bruijn family – and ϕ_i – the mean angle that the lines of this family make with $\boldsymbol{\delta}_i$. The vector $\boldsymbol{u}_i$ is given by the vector $\hat{\mathbf{e}}_i^{\parallel}$ rotated by the angle ϕ_i. The orientation $\boldsymbol{d}_i$ of a line of the family i is given by the average of the vectors $\mathbf{f}_j$ which define its tiles.

mean line spacing l_i is independent of the line family i. We shall calculate its common value shortly. The strain-free tiling's mirror symmetries guarantee that each angle $\phi_i = 0$. Deviations of l_i and ϕ_i from their strain-free values control nonzero values of $\mathbf{E}$ and determine the tile fractions n_{ij}. By definition, $l_i > 0$ and $-\pi/2 < \phi_i < \pi/2$.

Figure 5 represents lines of the ith family as sequences of tiles T_{ij}, each tile defined by the vector $\hat{\mathbf{e}}_i^{\parallel}$ and some other vector $\hat{\mathbf{e}}_j^{\parallel}$. Let $\boldsymbol{y}_0$ be the relative position of a given tile in a de Bruijn line, and follow this line in the plane. The position $\boldsymbol{y}_m - \boldsymbol{y}_0$ of the mth tile is the sum of the vectors defined by the successive edges of the tiles T_{ij} of the line between tile 0 and tile m. These vectors are *a priori* equal to $\pm\hat{\mathbf{e}}_j^{\parallel}$. Therefore we define $\mathbf{f}_j = \pm\hat{\mathbf{e}}_j^{\parallel}$ where the sign is chosen so that $\mathbf{f}_j \cdot \boldsymbol{\delta}_i > 0$. For large m, the number of tiles T_{ij} on any typical line is proportional to the tile fraction n_{ij}. The mean direction of this line is therefore

$$\boldsymbol{d}_i = \sum_{\substack{j=1 \\ j \neq i}}^{D} n_{ij} \mathbf{f}_j. \tag{2}$$

In general, a random tiling ensemble is completely characterized by $\{l_i\}$ and $\{\phi_i\}$. Since $D-2$ families of lines must be added to an original square lattice ($D=2$) to define a $D \to 2$ tiling we need $2(D-2)$ independent macroscopic parameters to characterize a tiling: l_i and ϕ_i for $i = 3, 4, \ldots, D$. Note that $2(D-2)$ is precisely the number of coefficients of the global phason gradient $\boldsymbol{E} = \nabla \bar{h}$. By comparison, in ref. 42, $4 \to 2$ tilings

are characterized by six tile concentrations d_{ij}, and two exact relations constrain them. Therefore these tilings are characterized by four independent parameters, as predicted above.

2.3.2. Relations Between Macroscopic Parameters

Consider now the tile fractions n_{ij} and their relation to $\{l_i\}$ and $\{\phi_i\}$. The tile number fractions n_{ij} are proportional to their density d_{ij} (number per unit area) via

$$n_{ij} = \frac{d_{ij}}{\sum_{k<l} d_{kl}}. \tag{3}$$

Conversely,

$$d_{ij} = \frac{n_{ij}}{\sum_{k<l} n_{kl} \sin|\pi(l-k)/D|}, \tag{4}$$

because the area of a tile T_{ij} equals $\sin|\theta^*_{ij}|$ where $\theta^*_{ij} = \pi(j-i)/D$ is the oriented angle between $\hat{\mathbf{e}}^{\parallel}_i$ and $\hat{\mathbf{e}}^{\parallel}_j$.

Note that θ^*_{ij} is also the angle between de Bruijn line directions i and j in a strain-free tiling. Generally speaking, throughout the text, starred quantities will refer to unstrained tilings with $\boldsymbol{E} = 0$.

Relation (2.3) is useful because the tile densities are given in a simple fashion by[42,46]

$$d_{ij} = |\boldsymbol{m}_i \times \boldsymbol{m}_j|, \tag{5}$$

where $\boldsymbol{m}_i$ (see Appendix A) is the parallel space gradient of the *ith* component of the smoothed membrane hyperspace coordinates. We also define a vector $\boldsymbol{u}_i$ for each line family: it is the unit vector along the shortest direction from one line of the family to the next; it is perpendicular to $\boldsymbol{d}_i$. Examining Fig. 5, if one travels a distance l_i in the direction $\boldsymbol{u}_i$, then one crosses one de Bruijn line of the family i on average and the ith component of the hyperspace coordinates increases by one on average. In contrast, if one travels any distance in the orthogonal direction $\mathbf{d}_i$, then the ith component of the hyperspace coordinates remains constant. Thus

$$\boldsymbol{m}_i = \frac{1}{l_i} \boldsymbol{u}_i \tag{6}$$

and Eq. (5) becomes

$$d_{ij} = \frac{1}{l_i l_j} |\boldsymbol{u}_i \times \boldsymbol{u}_j| = \frac{1}{l_i l_j} |\sin \theta_{ij}|, \tag{7}$$

where the angle between de Bruijn line directions

$$\theta_{ij} = \theta^*_{ij} + \phi_j - \phi_i. \tag{8}$$

Next we relate the distances $\{l_i\}$ and angles $\{\phi_i\}$ to the phason strain $\boldsymbol{E}$. Owing to relation (A.10) of Appendix A, we have

$$\boldsymbol{E} = \sum_{i=1}^{D} \frac{1}{l_i} \hat{\mathbf{e}}_i^{\perp} \otimes \boldsymbol{u}_i. \tag{9}$$

Defining $\boldsymbol{E}^2$ as the sum of the squares of the components of $\boldsymbol{E}$, then

$$\boldsymbol{E}^2 = \sum_{i=1}^{D} \sum_{j=1}^{D} \frac{1}{l_i l_j} (\boldsymbol{u}_i \cdot \boldsymbol{u}_j)(\hat{\mathbf{e}}_i^{\perp} \cdot \hat{\mathbf{e}}_j^{\perp}). \tag{10}$$

We prove in Appendix A that if $i \neq j$, then $\hat{\mathbf{e}}_i^{\perp} \cdot \hat{\mathbf{e}}_j^{\perp} = -2 \cos \theta^*_{ij}/(D-2)$. Hence

$$\boldsymbol{E}^2 = -\frac{2}{D-2} \sum_{i \neq j} \frac{1}{l_i l_j} \cos \theta_{ij} \cos \theta^*_{ij} + \sum_i \frac{1}{l_i^2}. \tag{11}$$

To determine the tile fractions n^*_{ij} and the mean line spacing l^*_i for strain-free tilings (we recall that starred quantities refer to unstrained tilings), remind that the tiling symmetry guarantees l_i is independent of i, and $\phi_i = 0$. Inspecting Eqs. (7) and (3), we may write $n_{ij} = C |\sin \theta^*_{ij}|$. To determine the normalization constant C, note that

$$1 \equiv \sum_{i<j} n^*_{ij} = C \sum_{0 \leqslant i < j < D} \sin \pi \frac{j-i}{D}. \tag{12}$$

In the limit of large D one then finds $C \simeq \pi/D^2$, so that

$$n^*_{ij} = \frac{\pi}{D^2} |\sin \theta^*_{ij}|. \tag{13}$$

The fraction n_i of tiles belonging to a given family i of lines, in a maximally symmetric tiling at large D,

$$n_i^* = \sum_{j \neq i} n_{ij}^* \simeq \frac{\pi}{D^2} \frac{2D}{\pi} = \frac{2}{D}, \tag{14}$$

allows us to compute the mean distance between de Bruijn lines of a given family. Since tiles of family i have, on average, the same area as tiles of the whole tiling, the above *numerical* tile fraction is also an *area* tile fraction. Since a fraction $2/D$ of tiles belong to lines of a family and the width of such a line is 1, the mean distance between lines is

$$l_i^* = D/2. \tag{15}$$

Setting $l_i = l_i^*$ and $\theta_{ij} = \theta_{ij}^*$ for all i and j in (11), we find again in a consistent way $\boldsymbol{E}^2 = 0$. Moreover, Eq. (7) implies

$$d_{ij}^* = \frac{4}{D^2} |\sin \theta_{ij}^*| = \frac{4}{\pi} n_{ij}^* \tag{16}$$

in the large D limit.

2.3.3. Miscellaneous Constraints

Geometrical considerations constrain the parameters $\{l_i\}$ and $\{\phi_i\}$. We describe a few such constraints here. The condition

$$\phi_{i-1} - \frac{\pi}{D} \leqslant \phi_i \leqslant \phi_{i+1} + \frac{\pi}{D} \tag{17}$$

imposes a certain regularity to the angles ϕ_i as a function of i. This constraint holds because lines of two consecutive families i and $i+1$ intersect only at a tile $T_{i,i+1}$, with edges $\hat{\mathbf{e}}_i^{\parallel}$ and $\hat{\mathbf{e}}_{i+1}^{\parallel}$ as displayed in Fig. 6. The oriented angles $(\boldsymbol{d}_i \boldsymbol{d}_{i+1})$ and $(\boldsymbol{\delta}_i \boldsymbol{\delta}_{i+1})$ have the same sign. Indeed, were these angles of opposite sign, no tile type could match at their intersection. As a consequence $(\boldsymbol{d}_i \boldsymbol{d}_{i+1}) = (\boldsymbol{\delta}_i \boldsymbol{\delta}_{i+1}) - \phi_i + \phi_{i+1} \geqslant 0$. Owing to $(\boldsymbol{\delta}_i \boldsymbol{\delta}_{i+1}) = \pi/D$, one gets $\phi_{i+1} - \phi_i \geqslant -\pi/D$ and condition (17) (see Fig. 6). Such conditions mean that at large D, when one adds a new family of lines in the iterative process, the angle ϕ_D is highly constrained by the pre-existing underlying tiling. For example, if a family $i = D$ is added in a strain-free tiling where $\phi_1 = \phi_{D-1} = 0$, the condition (17) reads $-\pi/D \leqslant \phi_D \leqslant \pi/D$.

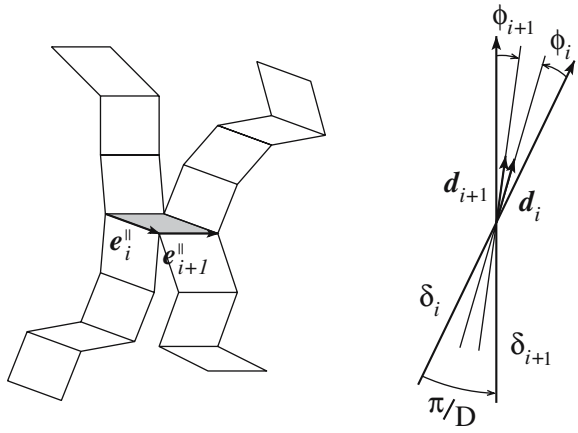

Fig. 6. Left: Intersection of two lines of two consecutive families i and $i+1$. Right: The corresponding directions $\boldsymbol{\delta}_i$, $\boldsymbol{\delta}_{i+1}$ (outer thick lines) and $\boldsymbol{d}_i$, $\boldsymbol{d}_{i+1}$ (inner thin lines). The vectors $\boldsymbol{d}_i$ and $\boldsymbol{d}_{i+1}$ are constrained by the condition $(\boldsymbol{d}_i\ \boldsymbol{d}_{i+1}) > 0$, which constrains in turn the angles ϕ_i and ϕ_{i+1}.

Since amongst the $2D$ parameters $\{l_i\}$ and $\{\phi_i\}$, only $2(D-2)$ are independent, there exist four relations between them. Of these four we will need this identity

$$\sum_{i<j} \frac{1}{l_i l_j} |\sin\theta_{ij}||\sin\theta_{ij}^*| = 1, \tag{18}$$

which reflects the fact that the total contribution of tile areas per unit area is by definition equal to 1. In other words, $\sum_{i<j} d_{ij}|\sin\theta_{ij}^*| = 1$ where d_{ij} is given by Eq. (7). This relation can also be derived from Eq. (4).

In the large D limit we have infinitely many tile species, so we expect that all $n_{ij} \to 0$. When taking the large D limit we wish to ensure that no finite fraction of tile species dominates, with tile fractions that are large compared to the remainder. Indeed, such a tiling would essentially be a finite D tiling, with a negligible number of defect tiles added in. Thus we introduce the notion of "bounded" relative fractions of tiles, which proves useful in discussing large D phason elastic constants. Consider tilings in which all tile fractions tend to 0 as $D \to \infty$, all vanishing at the same rate. Specifically, assume there exists $a > 0$ such that

$$n_{ij} \geqslant a\, n_{ij}^*, \tag{19}$$

holds uniformly for all i and j, which ensures that all tile fractions have the same order of magnitude as in strain-free tilings. Owing to Eq. (4), we could alternatively assume that there exists $b>0$ such that

$$d_{ij} \geqslant b\, d^*_{ij}. \tag{20}$$

Indeed, $\sum_{k<l} n_{kl}=1$ thus $\sum_{k<l} n_{kl} \sin|\pi(l-k)/D| \leqslant 1$ and $d_{ij} \geqslant n_{ij}$. Furthermore, $n_{ij} \geqslant a\, n^*_{ij} = \pi a/4\, d^*_{ij}$ and $b=\pi a/4$.

In addition, conditions (19) or (20) constrain the distances l_i and the angles θ_{ij} so that

$$l_i \leqslant c\, l^*_i, \tag{21}$$

where $c>0$ is a finite constant, and

$$|\sin\theta_{ij}| \geqslant d\, |\sin\theta^*_{ij}| \tag{22}$$

with $d>0$. Indeed, these two conditions together with Eq. (7) imply $d_{ij} \geqslant (d/c^2) d^*_{ij}$.

Comparable constraints can be stated in the membrane viewpoint, in which case the constraints appear as extreme allowed values of $\boldsymbol{E}$. Using (11) and constraint (21), one finds that the phason strain is vanishingly small at large D,

$$\boldsymbol{E}^2 \leqslant \frac{\text{Const.}}{D}. \tag{23}$$

The only way to achieve finite strain at large D is to allow a finite subset of the tile species to dominate. This large D behavior is related to our choice of normalizations of basis vectors both in $\mathcal{E}^\perp$ and in $\mathcal{E}^\parallel$. Our choice is consistent with current practice for finite D tilings.

3. MEAN-FIELD THEORY, CORRELATIONS AND FINITE D CORRECTIONS

This section applies the iterative construction of Section 2.2, to develop a mean-field theory of strain-free random tilings. We first propose a close upper-bound of $\log 2$ for the entropy per tile, which can be seen as the order 0 of the mean-field theory developed below. We then refine the estimate by calculating, within mean-field theory, the distribution of tile vertex types. Finally, we explore spatial correlations and related issues.

3.1. First Entropy Estimate

Here we set the upper-bound of $\log 2$ for the entropy. To begin with, we mention that rigorous bounds of the large D entropy are known in the case of *fixed-boundary tilings of unitary side length* (see paper II,[36] Section 2):

$$\frac{1}{3}\log 2 \leqslant \sigma_{\infty}^{\text{fixed}} \leqslant 1.44 \log 2. \tag{24}$$

Since it is demonstrated in the same reference that this entropy per tile is equal to the free-boundary large D entropy σ_{∞}, the same bounds should hold for σ_{∞}. Our first mean-field estimate $\log 2$ belongs to this interval, as well as the refined mean-field estimate of Section 3.2.

Let $P_D(N_D)$ denote the number of ways to follow a directed walk of family D on a $D \to 2$ tiling. N_D is the total length of a single walk, or the cumulative length of a few walks. We will neglect contacts among walks of family D, which is justified since $l_i \sim D$. To calculate a typical value of $P_D(N_D)$, consider the problem of constructing bottom-to-top paths on a typical tiling. At each step, the path may follow one or more routes (Fig. 7). The only requirement is that the path segment leading out of a vertex must contain an upwards component. We estimate the number of

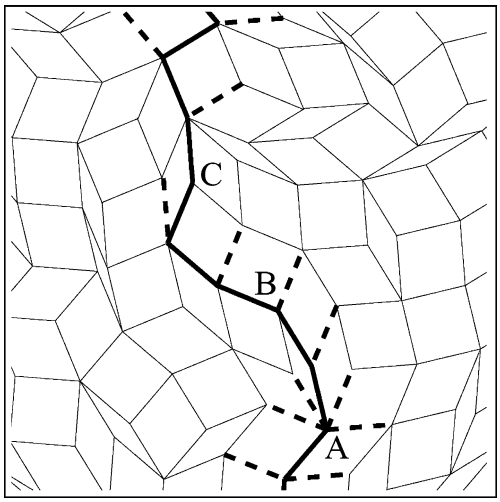

Fig. 7. A random path (thick line) on a tiling as a succession of vertices with choices (dashed edge = choice not taken). There are five choices at vertex A (*i.e.* $N_c(\mathrm{A}) = 5$), two choices at vertex B and only one choice at vertex C.

paths as the product over vertices v of the number of choices $N_c(v)$ to be made at each step

$$P_D(N_D) \approx \prod_{v=1}^{N_D} N_c(v). \tag{25}$$

Evaluation of Eq. (25) requires the distribution of values $N_c(v)$ along paths. Because we do not know this distribution (yet), we settle for an estimate that yields an upper bound on $P_D(N_D)$, and eventually on the entropy per tile S_D. Note that the product in Eq. (25) is the N_Dth power of the geometric mean of $N_c(v)$. The geometric mean of any set of positive numbers is bounded above by the arithmetic mean, reaching this bound only when all values are equal. The arithmetic mean $\bar{N}_c = \bar{Z}/2$, with $\bar{Z}$ the mean coordination number (or degree), because on average half the tile edges at each vertex have a vertical component in the northerly direction. From Euler's theorem applied to infinite rhombus tilings, we know $\bar{Z} = 4$, so that $\bar{N}_c = 2$. We deduce the D-independent upper bound

$$P_D(N_D) \leqslant 2^{N_D}. \tag{26}$$

Let B_D be the number of $D \to 2$ tilings (free boundary tilings of some size $\mathcal{R}$). Since each $D+1 \to 2$ tiling is in one-to-one correspondence with random walks on a $D \to 2$ tiling,

$$B_{D+1} \approx P_D(N_D) B_D. \tag{27}$$

We iterate this relationship to write

$$B_D = \prod_{D'=3}^{D-1} P_{D'}(N_{D'}). \tag{28}$$

Inserting relation (26) for the path counting, we find

$$B_D \leqslant 2^{N_3 + \cdots + N_{D-1}}. \tag{29}$$

Since the number of tiles is $N = \sum_{D'} N_{D'}$, we obtain the entropy per tile

$$\sigma_D = \frac{\log B_D}{\sum N_{D'}} \leqslant \log 2 = 0.693. \tag{30}$$

The limiting entropy σ_∞ is bounded above by $\log 2$.

3.2. Refined Mean-field Calculations

The entropy value $\log 2$ just derived is not exact for two reasons. First, to properly compute the geometric mean of N_c we need the full vertex path choice probability distribution $\pi(N_c)$. Second, our estimate Eq. (25) neglected correlations among the numbers of choices at different steps along the path. In this section, we address the first point. In the next one we shall address briefly the second point.

Following the logic in Section 3.1, the limiting entropy is

$$\sigma_\infty = \lim_{D\to\infty} \lim_{k\to\infty} \frac{\log P_D(k)}{k}, \tag{31}$$

where $P_D(k)$ is the number of k-step paths on a $D \to 2$ tiling. The mean-field approximation assumes that the steps of such paths are uncorrelated so that the number of paths is given by Eq. (25). The vertices v belong to a random $D \to 2$ tiling. Therefore the numbers of choices $N_c(v)$ are distributed according to a probability distribution $\pi_D(N_c)$. When D tends to infinity, this distribution tends toward a limiting distribution, denoted by $\pi(N_c)$. Thus, after a short calculation, Eqs. (31) and (25) become

$$\sigma_\infty^{MF} = \sum_{N_c=1}^{\infty} \pi(N_c) \log N_c. \tag{32}$$

To get the mean-field distribution $\pi(N_c)$, let us first denote by $\pi_D(q, p)$ the fraction of vertices on a $D \to 2$ random tiling with q in-coming edges ("legs") and p out-going ones ("arms") (see Fig. 8). Neglecting correlations, a (q, p)-vertex v of a $D \to 2$ tiling will be visited by paths with probability $\pi_D(q, p)$ and will then give birth to two vertices v_1 and v_2, as illustrated in Fig. 8. These latter vertices belong to a $D+1 \to 2$ tiling. Each leg and each arm of v will be chosen with probabilities $1/q$ and $1/p$, respectively. The new edge from v_1 to v_2 is arbitrarily chosen to be oriented upward in the $D+1 \to 2$ tiling and is therefore an arm for v_1 and a leg for v_2.

Indeed, a vertex with p' arms and q' legs can be either the "left-son" v_1 or the "right-son" v_2 of a "father-vertex" v in a $D \to 2$ tiling (Fig. 8). The two son vertices together inherit all their father's arms and legs, plus an extra arm and leg (for the path along which the vertex is split). Finally, in addition, the left son gets an extra arm and the right son an extra leg from the new bond that joins them. Consequently the left-son has more than one arm and the right-son has more than one leg.

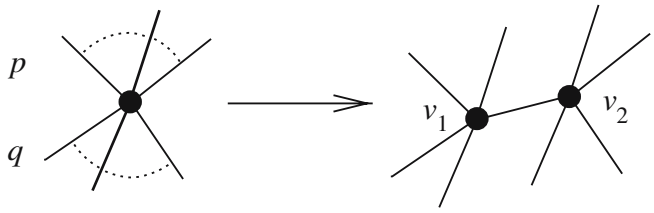

Fig. 8. A path going through a vertex v of a $D \to 2$ tiling gives birth to two vertices v_1 and v_2 of a $D+1 \to 2$ tiling. The path follows any leg of v with probability $1/q$ and any arm with probability $1/p$.

As a consequence, in this mean-field approximation, the probabilities $\pi_{D+1}(q, p)$ can be written as linear combinations of the probabilities $\pi_D(q, p)$. The corresponding linear operator will be denoted by $\mathcal{A}:\pi_D \mapsto \pi_{D+1}$. It is infinite-dimensional since q and p can be arbitrarily large when D goes to infinity. The operator $\mathcal{A}$ is defined by

$$\pi_{D+1}(q', p') = (1-\delta_{q',1}) \sum_{\substack{q \geqslant q'-1 \\ p \geqslant p'}} \frac{\pi_D(q, p)}{2qp} + (1-\delta_{p',1}) \sum_{\substack{p \geqslant p'-1 \\ q \geqslant q'}} \frac{\pi_D(q, p)}{2qp}. \tag{33}$$

The first and second term refer, respectively, to left- and right-sons (v_1 and v_2). The factors of $1/2$ expresses that a vertex is either a left-son or a right-son with probability $1/2$. Moreover, each arm-leg pair is chosen with probability $1/pq$ among all possibilities (see Fig. 8). The limiting distribution $\pi(q, p)$ is the fixed point of $\mathcal{A}$, the eigenvector with eigenvalue 1.

The diagonalization of $\mathcal{A}$ being rather complex, we focus on a summation of the previous relation on legs q. This yields a recursion relation on the arm statistics, in other words on the choice statistics

$$\pi_D(N_c) = \sum_{q=1}^{\infty} \pi_D(q, N_c). \tag{34}$$

We denote this operator by $\hat{\mathcal{A}}$ and write it in matrix form, where rows and columns are indexed by N_c, as

$$\hat{\mathcal{A}} = \begin{pmatrix} \frac{1}{2}1 & \frac{1}{2}\frac{1}{2} & \frac{1}{2}\frac{1}{3} & \frac{1}{2}\frac{1}{4} & \frac{1}{2}\frac{1}{5} & \cdots \\ \frac{1}{2}1 & \frac{1}{2} & \frac{1}{3} & \frac{1}{4} & \frac{1}{5} & \cdots \\ 0 & \frac{1}{2}\frac{1}{2} & \frac{1}{3} & \frac{1}{4} & \frac{1}{5} & \cdots \\ 0 & 0 & \frac{1}{2}\frac{1}{3} & \frac{1}{4} & \frac{1}{5} & \cdots \\ 0 & 0 & 0 & \frac{1}{2}\frac{1}{4} & \frac{1}{5} & \cdots \\ 0 & 0 & 0 & 0 & \frac{1}{2}\frac{1}{5} & \cdots \\ \vdots & \vdots & \vdots & \vdots & & \ddots \end{pmatrix}. \tag{35}$$

This operator preserves the mean number of choices $\langle N_c \rangle = 2$. The fixed point is

$$\pi(N_c) = \frac{1}{\sqrt{e}} \frac{2N_c - 1}{2^{N_c}(N_c - 1)!}. \tag{36}$$

The first few values of $\pi(N_c)$ are listed in Table IV, where they may be compared with Monte Carlo simulation results (see paper II[36]). The values peak at $N_c = 2$ and decrease rapidly for large N_c.

The mean-field entropy in Eq. (32) becomes

$$\sigma_\infty^{MF} = \frac{1}{\sqrt{e}} \sum_{N_c=1}^{\infty} \frac{2N_c - 1}{2^{N_c}(N_c - 1)!} \log N_c \simeq 0.598. \tag{37}$$

This mean-field value is satisfactorily close to the numerical value obtained by Monte Carlo simulations (see paper II[36]), namely $\sigma_\infty \simeq 0.568$, and is well below the upper bound $\log 2 = 0.693$.

Table IV. The first values of the limiting distribution $\pi(N_c)$, obtained both in the mean-field approximation Eq. (36) and numerically, by Monte Carlo simulations (from paper II[36])

N_c	1	2	3	4	5
$\pi(N_c)$ (Mean-field)	0.30	0.45	0.19	0.04	0.007
$\pi(N_c)$ (Numerical)	0.26	0.51	0.21	0.03	0.001

3.3. Spatial Correlations

Spatial correlations play a crucial role in two-dimensional finite codimension tilings since they are critical systems with long-range correlations.[21] In particular, they condition the diffusive behavior of de Bruijn lines, they constrain the successive steps in the iterative construction process, and they reduce the entropy slightly below the mean-field value. We can calculate both short- and long-range correlations among p and q within our mean-field theory. We also note some expected properties of perpendicular space height correlations.

3.3.1. Short-Ranged Correlations

Consider the short-ranged correlation between the numbers of arms and legs p and q on individual vertices. Within the mean-field approximation, $\langle pq\rangle_D = \sum_{p,q} \pi_D(q,p)pq$. If, at step D, a vertex v has p arms and q legs (see Fig. 8), then its first son v_1 has on average $(2+3+\cdots(p+1))/p = (p+3)/2$ arms independently of its number of legs, and $(1+\cdots+q)/q = (q+1)/2$ legs independently of its number of arms. Similarly, its second son v_2 has on average $(p+1)/2$ arms and $(q+3)/2$ legs. Therefore

$$\begin{aligned}\langle pq\rangle_{D+1} &= \sum_{p,q} \pi_D(q,p)\left(\frac{1}{2}\,\frac{p+1}{2}\,\frac{q+3}{2} + \frac{1}{2}\,\frac{p+3}{2}\,\frac{q+1}{2}\right) \\ &= \frac{1}{4}(\langle pq\rangle_D + 11),\end{aligned} \tag{38}$$

since $\langle p\rangle_D = \langle q\rangle_D = \langle N_c\rangle_D = 2$. The limiting value is $\langle pq\rangle_\infty = 11/3$. Moreover, distribution (36) leads to $\Delta p = (\langle p^2\rangle_\infty - \langle p\rangle_\infty^2)^{1/2} = \sqrt{3}/2$ and $\Delta p = \Delta q$. Therefore the mean-field covariance of p's and q's is

$$\mathrm{cov}(p,q) = \frac{\langle pq\rangle_\infty - \langle p\rangle_\infty\langle q\rangle_\infty}{\Delta p\,\Delta q} = -4/9 \simeq -0.44, \tag{39}$$

also in good agreement with the numerical value $\mathrm{cov}(p,q) \simeq -0.36$ (see paper II[36]). The main contribution to those correlations comes from the asymmetry caused by the edge between v_1 and v_2.

We can use the covariance to improve on our original "upper bound" entropy estimate Eq. (30) of $\log 2 = 0.693$. Whereas the original estimate arose from the mean number of choices in single steps, we can instead consider the geometric mean number of ways to make two steps. The product pq counts the number of two-step paths passing through a given vertex. Hence an improved entropy estimate is $\log\sqrt{11/3} = 0.649$, which

is indeed closer to the numerical value of 0.568, though nowhere near as close as our full mean-field value in Eq. (37). Ideally, we would determine the full distribution of choices (i.e. number of arms) in two-step paths, $\pi_2(N_c^1, N_c^2)$ then we could replace our MFT estimate Eq. (37) with

$$\sigma_\infty^{MF2} = \sum_{N_c^1, N_c^2 = 1}^{\infty} \pi_2(N_c^1, N_c^2) \log \sqrt{N_c^1 N_c^2}, \tag{40}$$

which should improve upon the value in Eq. (37) just as $\log\sqrt{11/3}$ improved upon $\log 2$. Unfortunately, it is considerably more difficult to obtain $\pi_2(N_c^1, N_c^2)$ than $\pi(N_c)$.

3.3.2. Long-Ranged Correlations

To calculate long-range correlations using our iterative construction method, two phenomena compete: de Bruijn lines running through a tiling destroy vertex-to-vertex correlations, while they increase distances between vertices. Consider two vertices separated by a distance u_n on an $n \to 2$ tiling. The addition of successive families of lines to get higher codimension tilings ($D \to 2$ with $D > n$) make the tiling "swell" homogeneously, and the distances grow like D. When D increases, the distance between the two vertices increases so that

$$u_D / D \simeq u_n / n. \tag{41}$$

The idea is now to track such pairs of vertices, and to estimate how their correlation functions evolve at the same time they are moving apart.

To track these correlation functions as D increases, we estimate correlations between the number of choices at vertices, $N_c(v)$. Define the correlation function between vertices v_a and v_b, widely separated in space,

$$\begin{aligned} C_n(r) &= \frac{1}{N_P} \sum_{d(v_a, v_b) = r} N_c(v_a) N_c(v_b) - \left(\frac{1}{N_v} \sum_v N_c(v) \right)^2 \\ &= \langle N_c(v_a) N_c(v_b) \rangle_r - \langle N_c \rangle^2. \end{aligned} \tag{42}$$

The first average runs over the N_P pairs of vertices of $n \to 2$ tilings separated by a distance r. The second average runs over all N_v vertices in

the tiling. In the following, we denote $\langle N_c(v_a)N_c(v_b)\rangle_r = \gamma_n$. Moreover, the mean number of choices $\langle N_c\rangle = 2$, so that

$$C_n(r) = \gamma_n - 4. \tag{43}$$

When a new line passes through either v_a or v_b, their correlation diminishes. Each vertex has a probability $2/n$ that a new line goes through it (see Eq. (14)). Therefore the probability that either one of the pair (v_a, v_b) will be affected by a new line is $4/n$. A fraction $1-4/n$ of pairs separated by r are unaffected, so their correlation remains equal to γ_n. The remaining pairs *are* affected, and we denote their new correlation by γ_n' which we now calculate.

Each pair (v_a, v_b) that is affected gives birth to two pairs. One of its vertices, say v_b, remains unchanged while the other one, v_a, gives birth to two vertices, a "left-son" v_{a1} and a "right-son" v_{a2} (see Fig. 8). On average,

$$N_c(v_{a1}) = \frac{1+2+\cdots+N_c(v_a)}{N_c(v_a)} = N_c(v_a)/2 + 1/2 \tag{44}$$

and $N_c(v_{a2}) = N_c(v_a)/2 + 3/2$, since a right-son has one more arm than a left-son. Therefore, averaging on the whole tiling, we find

$$\gamma_n' = 1/2(\langle N_c(v_{a1})N_c(v_b)\rangle + \langle N_c(v_{a2})N_c(v_b)\rangle) = \gamma_n/2 + 2. \tag{45}$$

Now we estimate γ_{n+1}, the correlation averaged over all tiling vertices after the introduction of the lines of family $n+1$. For original vertices *not* touched by the new lines, the correlation remains γ_n. For original vertices that *are* touched by the new lines, the correlation becomes γ_n'. Therefore,

$$\gamma_{n+1} = \frac{(1-4/n)\gamma_n + 8/n\,\gamma_n'}{(1-4/n)+8/n} \approx (1-8/n)\gamma_n + 8/n\,\gamma_n' + \mathcal{O}(1/n). \tag{46}$$

Hence

$$C_{n+1}(u_{n+1}) = (1-4/n)C_n(u_n). \tag{47}$$

Now iterating from $n \to D$ we write

$$C_D(u_D) = C_n(u_n) \prod_{k=n+1}^{D} (1-4/k). \tag{48}$$

For large n and D,

$$\log C_D = \log C_n + \sum_{k=n}^{D-1} \log(1-4/k)$$
$$\simeq \log C_n - 4 \sum_{k=n}^{D-1} 1/k \simeq \log C_n - 4\log(D/n) \tag{49}$$

from which it follows that

$$D^4 C_D(u_D) \simeq n^4 C_n(u_n). \tag{50}$$

Using Eq. (41) we have

$$(u_D)^4 C_D(u_D) \simeq (u_n)^4 C_n(u_n). \tag{51}$$

and finally

$$C_\infty(r) \simeq \text{const.} \frac{1}{r^4}. \tag{52}$$

This expression holds only for large values of r, since we do not take into account the discreteness of tilings at very short range. Correlations fall off rapidly at large distance.

3.3.3. Height-Height Correlations

In two dimensions, the random tiling hypothesis Eq. (1) imples logarithmic behavior of the two-point height-height correlation function[5]

$$G(r) \equiv \langle (h(r) - h(0)^2 \rangle = \frac{1}{\pi K} \log r \tag{53}$$

in the large r limit. We give here the generic form, without regard to the specific components of our $D-2$ dimensional height function or the particular irreducible components of the phason strain tensor $\mathbf{K}$. The only requirement is that the elasticity tensor be positive definite, i.e. $K > 0$. Presumably Eq. (53) will hold for any finite D.

We can easily derive an alternative formula for $G(r)$ in the limit $r \ll D$. Consider the shortest path joing two tiling vertices, and let s be the number of tile edges on this path. Provided $s \ll D$, a typical path contains

s distinct edge orientations $\pm\hat{\mathbf{e}}_i^{\parallel}$ and its length r is proportional to s. In the perpendicular space, $h(s)-h(0)$ contains s distinct terms equaling $\pm\hat{\mathbf{e}}_i^{\perp}$, the remaining $D-2-s$ components equaling 0. Since the products (A.6) are of order at most $1/D$ whereas $(\hat{\mathbf{e}}_i^{\perp})^2=1$, $(h(s)-h(0))^2\simeq s$ when $s\ll D$. Consequently

$$G(r)\propto r \tag{54}$$

for $r\ll D$. Now taking the $D\to\infty$ limit, and comparing Eq. (54) with the large r limit (53), we see that K must vanish in the limit of large D or else $G(r)$ will lack monotonicity. Section 4.2 provides further evidence for the vanishing of K.

3.4. Finite D Corrections

The mean-field calculations of Section 3.2 neglect the fact that at the step D of the iterative process, only a diminishing fraction of of the vertices are visited by paths. Correcting this oversight does not alter the fixed point of the process, but predicts finite D corrections to it. Indeed, at step D, a fraction $2/D$ of the vertices are visited. Each of them has two sons and Eq. (33) applies only to a fraction of new vertices of order $4/D$ when one iterates at step D. The remaining vertices are unaffected. Hence the correct evolution operator is

$$\hat{\mathcal{A}}_D=\frac{4}{D}\hat{\mathcal{A}}+\left(1-\frac{4}{D}\right)\mathrm{Id}. \tag{55}$$

where $\hat{\mathcal{A}}$ is the operator introduced in Eq. (35). For any finite D, the fixed point of $\hat{\mathcal{A}}$ remains the fixed point of $\hat{\mathcal{A}}_D$. Any eigenvector e of $\hat{\mathcal{A}}$ associated with the eigenvalue μ evolves as follows:

$$\begin{aligned}\hat{\mathcal{A}}_D\hat{\mathcal{A}}_{D-1}\ldots\hat{\mathcal{A}}_2\cdot e&=\prod_{k=2}^{D}\left(\frac{4}{k}\mu+\left(1-\frac{4}{k}\right)\right)e\\&=\prod_{k=2}^{D}\left(1+\frac{4(\mu-1)}{k}\right)e\simeq\frac{C}{D^{4(1-\mu)}}\,e,\end{aligned} \tag{56}$$

where C is some constant of order 1, using the same calculation scheme as in Eqs. (49) and (50).

Hence we get power-law convergence towards the fixed point instead of exponential convergence. The spectrum of $\hat{\mathcal{A}}$ can be calculated numerically, by taking finite but larger and larger approximations of $\mathcal{A}$. The spectrum converges rapidly towards $\{1, 1/2, 1/3, \dots, 1/p, \dots\}$. Eigenvalue $\mu = 1$ is the desired fixed point. The slowest mode corresponds to $\mu = 1/2$ and to a $1/D^2$ behavior of the finite D corrections to $\pi(N_c)$, and therefore to the entropy (32). Thus finite D corrections to the entropy associated with path-counting are expected to behave like $1/D^2$ in the mean-field approximation.

4. DE BRUIJN LINE INTERACTIONS

The mean-field theory addresses the statistics of isolated de Bruijn lines influenced by the statistics of the $D-1 \to 2$ tiling they meander on, but with no other interactions. A crucial fact about the de Bruijn line construction of tilings is that lines within the same family may never cross, resulting in an effective repulsive interaction at contact.[47] We now analyze the effect of interactions on finite size corrections and on phason elasticity.

4.1. Entropy Loss Due to Contacts in Strain-free Tilings

We call "contact" between two neighbor lines of a same family a configuration where these lines are adjacent. Such a situation is represented in Fig. 4, where we have circled one contact between neighboring paths (or de Bruijn lines). If we follow the lines in the direction t, the local initial angles θ and θ' they make with their global direction $\boldsymbol{\delta}$ after the contact are constrained by the noncrossing relation $\theta \leqslant \theta'$. This constraint divides the number of allowed configurations by a factor of order 2 as compared to the free path case, and reduces the total entropy by about $\log 2$.

To estimate the global entropy loss due to contacts in an infinite tiling, we must calculate the density of contacts. A crucial quantity is the distance L_i between consecutive contacts with neighboring lines of family i. Inspecting Fig. 4 we see that contacts between lines of family $i = D$ result from diffusion of the lines in the direction $\hat{\mathbf{e}}_D^{\parallel}$. Note that L_i depends on both l_i (because wider separation reduces the frequency of contacts of diffusing lines) and ϕ_i (because the diffusion constant has corrections in the ϕ_i; these corrections are quadratic because of the symmetry of the problem through any line). In strain-free tilings, which have maximal rotational symmetry, $l_i = l_i^* = D/2$ and $\phi_i = 0$ and $L_i = L$ is independent of i.

Define the diffusion constant $\mathcal{D}$ so that the lateral displacement u after traveling a distance L in the direction δ_i is $u^2 \sim \mathcal{D}L$. We presume that $\mathcal{D}$ takes a finite limiting value in the large D limit. Thus $\mathcal{D}L \sim (l_i^*)^2$,

and there is approximately one contact among lines of family i in every region of area $\mathcal{A}=l_i^* L=(l_i^*)^3/\mathcal{D}$. Adding up the total number of contacts expected among lines of all orientations, we estimate the loss of entropy per unit area as

$$\Delta\sigma \approx -\frac{\mathcal{D}D}{(l_i^*)^3}\log 2 = -8\mathcal{D}\log 2\frac{1}{D^2}. \tag{57}$$

This quantity should be suitably rescaled if one is interested in the entropy per tile. The strain-free loss of entropy falls off like $1/D^2$ because as D grows large, lines of like orientation rarely contact each other.

4.2. Phason Elastic Constant Tensor

We now investigate the phason strain dependence of the entropy and test the generic form assumed in Eq. (1). A thorough discussion of phason elasticity requires a group-theoretical analysis of rotational invariants,[44] each leading to an independent phason elastic constant, which lies beyond the scope of this paper. Rather, we will assume a generic form of strain and estimate its impact on the entropy. In particular, we shall see that $\mathbf{K}$ decays like $1/D$ when D becomes large.

To start, consider expanding $\sigma_D(\boldsymbol{E})$ to second order in ϕ_i and $\delta l_i = l_i - l_i^*$. Note that this expansion does not couple explicitly angles ϕ_i and line spacings δl_i because a symmetry through any line changes ϕ_i into $-\phi_i$ whereas it does not affect δl_i. Therefore this expansion is the sum of a quadratic form in the ϕ_i's and of a quadratic form in the δl_i's. Some phason elastic constants are related to the angles ϕ_i only. The remaining ones are related to the variations of the line spacings l_i only.

At present we consider only the l_i strain. To estimate the strain-dependence of the loss of entropy by contact we must calculate the density of contacts as a function of strain. We impose a global phason strain by varying only the mean distance l_i between de Bruijn lines of family i. Let

$$l_i = l_i^*(1+\lambda\delta_i) \tag{58}$$

where λ is a small parameter that controls the strength of the phason strain. Here δ_i is an arbitrary but bounded function of i whose mean and standard deviation obey $\langle\delta\rangle = 0$ and $\langle\delta^2\rangle = 1$, where the averages are taken over families i. Owing to the bounded tile fraction constraint Eq. (21), whatever the strength of the phason strain, l_i is of order D and λ is of order at most 1. The requirement of vanishing mean is imposed by the normalization condition (18).

Consider a pair of adjacent lines of family i, and evaluate L_i, the mean distance between contacts of these lines. Thus $\mathcal{D}L_i \sim l_i^2$, and there is approximately one contact among lines of family i in every region of area $\mathcal{A}_i = l_i L_i = l_i^3/\mathcal{D}$. The entropy loss (57) becomes

$$\Delta\sigma \approx -\mathcal{D}D\langle l^{-3}\rangle \log 2. \tag{59}$$

Now consider the average $\langle l^{-3}\rangle$. For vanishing phason strain ($\lambda \to 0$), Eq. (15) reveals that $l_i = l_i^* = D/2$. Expanding l_i^{-3} in Eq. (58) for small λ, using the known mean and standard deviation of δ_i, we obtain

$$\langle l^{-3}\rangle \approx \left(\frac{2}{D}\right)^3 (1+6\lambda^2). \tag{60}$$

Substituting this expression into Eq. (59) yields

$$\Delta\sigma \approx -\left(\frac{1}{D^2} + \frac{6\lambda^2}{D^2}\right) 8\mathcal{D}\log 2. \tag{61}$$

We find two terms, each falling off as $1/D^2$. The first term, which arises in the absence of strain, reproduces Eq. (57). In a strained tiling with $\lambda \neq 0$, owing to Eq. (21), l_i remains of order D, and the loss of entropy is also of order $1/D^2$. Although the frequency of contacts increases due to the strain, it still falls off for large D.

Because the entropy is independent of the phason strain at the large D limit, we again conclude that the phason elastic constant vanishes. We have seen (Eq. (23)) that for bounded tile fractions the phason strain $\boldsymbol{E}^2$ decreases like $1/D$ as D increases. Comparing Eq. (1) with the strain-corrections of order $1/D^2$ that we can calculate, we conclude that the phason elastic tensor $\mathbf{K}$ falls off as $1/D$.

We can understand the vanishing phason strain correction by the following qualitative argument. Consider a domain of the tiling of diameter Δ, large as compared to the tile size 1 but small as compared to the mean distance between two lines of a same family, $1 \ll \Delta \ll D$. For example, one can choose $\Delta = \sqrt{D}$. In such a domain there is *at most* one de Bruijn line per family, and no lines at all of most families. Since Δ tends to infinity with D, the area of the domain tends to infinity and the number of lines and tiles in the domain also tend to infinity.

Locally, as D and Δ go to infinity, the tiling looks like a large co-dimension $D' \to 2$ tiling (where $D' \sim \Delta$), with only one line per family (see Fig. 9). The entropy per tile in this domain tends towards a quantity

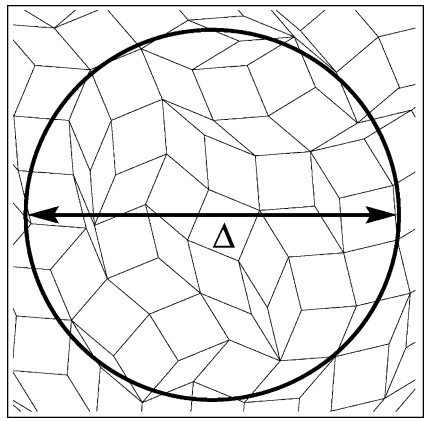

Fig. 9. A domain of diameter Δ which contains at most one de Bruijn line per family.

σ_{loc} which depends neither on the strain nor on the domain under consideration and is directly related to a simplified problem with one line in each family. The global entropy per tile σ_∞ is the average over the whole tiling[11] of the local entropy density σ_{loc}. Therefore $\sigma_\infty = \sigma_{\text{loc}}$ is independent of the de Bruijn line separations l_i, of the angles ϕ_i and of the global phason strain.

5. TILINGS OF DIMENSION OTHER THAN 2

This section discusses briefly cases of dimension other than $d=2$. The high codimension $d=1$ case is especially interesting because it is exactly solvable. It serves as an excellent illustration of several of the concepts in the paper and contrasts interestingly with the high codimension $d=2$ case. We then present results and conjectures for the high codimension $d=3$ case and the codimension 1 case with $d=D-1$ for arbitrary d.

5.1. $D \to 1$ Tilings

One-dimensional high codimension $D \to 1$ tilings are exactly solvable, as we show it in this section. The special case $D=2$ was previously discussed, for example in.[5] These tilings comprise D different species of tiles randomly arranged on a line. This case is unusual since the entropy per tile tends to infinity with D. Still, this example is quite instructive since it already contains a characteristic feature of large codimension tilings: when D goes to infinity, we prove that the entropy no longer depends on the relative tile fractions provided these quantities remain bounded.

The number of tilings is given by the multinomial coefficient:

$$W^{D\to 1}(k_1,\dots,k_D)=\frac{(k_1+k_2+\cdots+k_D)!}{k_1!k_2!\dots k_D!}. \tag{62}$$

Introducing tile fractions $x_i=k_i/(k_1+\cdots+k_D)$, we get the entropy per tile at large D

$$\sigma^{D\to 1}=-\sum_{i=1}^{D}x_i\log x_i. \tag{63}$$

This entropy is maximal at $x_i=1/D$ where it equals $\log D$. In one dimension, for the sake of convenience in the calculation, we set the upper bound $x_i\leqslant a/D$ where $a>0$ to prevent some tile species from being dominant. Then $-\log x_i\geqslant\log D-\log a$, and hence $-\sum_{i=1}^{D}x_i\log x_i\geqslant\log D-\log a$ because $\sum_{i=1}^{D}x_i=1$. Therefore

$$\log D-\log a\leqslant\sigma^{D\to 1}\leqslant\log D. \tag{64}$$

The entropy grows asymptotically like $\log D+\mathcal{O}(1)$, independently of the exact tile fractions provided they remain bounded.

Large D phason elastic constants can also be calculated. Near the entropy maximum at $x_i=1/D$,

$$K_i=\frac{\partial^2\sigma}{\partial x_i^2}=-D. \tag{65}$$

Let $x_i=\frac{1}{D}+\delta x_i$, so that $\sigma=\sigma_{\max}-\frac{D}{2}\sum\delta x_i^2$. The average gradient of the function h (representing the one-dimensional membrane in the D-dimensional space) is characterized by the average angle ψ this membrane makes with the reference direction $(1,1,\dots,1)$. Specifically, $(\nabla h)^2=\tan^2\psi\simeq\psi^2$. Now,

$$1-\frac{\psi^2}{2}\simeq\cos\psi=\left(D\sum_{i=1}^{D}x_i^2\right)^{-1/2}\simeq 1-\frac{D}{2}\sum_{i=1}^{D}\delta x_i^2. \tag{66}$$

Finally, $(\nabla h)^2=D\sum\delta x_i^2$ and

$$\sigma^{D\to 1}\simeq\sigma_{\max}-\frac{K}{2}(\nabla h)^2, \tag{67}$$

where the phason elastic constant $K = 1$ is vanishingly small as compared to the entropy $\sigma_{\max}$. Note the value of K is independent of D, and of course it agrees with the previous value[5] derived for $D = 2$.

5.2. $D \to 3$ Tilings

Unlike the cases of $d = 1$ and $d = 2$, we have neither exact, nor extensive numerical information available for high codimension $d = 3$ tilings. Table II collects available data on $d = 3$ strain-free boundary tilings. For $D \leqslant 3$ the entropy vanishes. No data is available for $D = 5$. For $D = 4$ and 6, data is available from computer simulations.[48,49] The $6 \to 3$ case[49] deals with rhombohedron tilings with icosahedral symmetry.

To estimate the large D limit, we insert oriented membranes into $d = 3$ tilings, as previously we inserted lines into $d = 2$ tilings. Membranes of like orientation are forbidden to cross. In the large D limit, we can neglect contact of like-oriented membranes and consider the statistics of a single membrane in generic high symmetry tilings. Let $M_D(\tau)$ denote the number of such membranes that can be inserted into tiling τ and $\bar{M}_D$ be the arithmetic mean of this number. We find that the number of $D \to 3$ tilings is

$$B_D = \prod_{D'=3}^{D-1} \bar{M}_{D'}. \tag{68}$$

analogously to Eq. (28). The entropy per tile is the logarithm of this number divided by the number of tiles.

We obtain an upper bound on the large D entropy of $d = 3$ tilings in a manner similar to our upper bound of $\log 2$ for for $d = 2$. Recall 2^D is an upper bound on the number of directed paths in $d = 2$ tilings, and is actually realized only on special tilings in which the degree $Z = 4$ at all sites, with two incoming and two outgoing vertices. Similarly, the number of directed membranes may be maximal on a special tiling in which the coordination number and choice numbers are most homogeneous. This is the simple cubic tiling in which each vertex is six-fold coordinated. The membrane orientation should be in the plane perpendicular to the (111) axis. At each vertex there are 18 possible directed membrane configurations. This leads to $\bar{M}_D \leqslant 18^N$ membranes containing N rhombi, a substantial overestimate because many of these configurations force unique membrane structures nearby.

A true upper bound is

$$\bar{M}_D \leqslant e^{\sigma_{3\to 2} N}, \quad \sigma^{D\to 3} \leqslant \sigma^{3\to 2}, \tag{69}$$

because the problem of the directed membrane on the simple cubic lattice is just the $3 \to 2$ tiling problem. This value is an upper bound because it neglects contacts, and because generic $D \to 3$ tilings will be less homogeneous than the simple cubic lattice and therefore the entropy lower.

5.3. $D \to D-1$ Tilings

In this section, we study the entropy of strain-free $D \to D-1$ tilings where the D different tiles appear with the same fraction $1/D$ and we derive rigorous lower and upper bounds:

$$\frac{\log 2}{D} \leqslant \sigma^{D \to D-1} < \frac{3\sigma^{3\to 2}}{D} \tag{70}$$

Note that the two prefactors $\log 2 \simeq 0.693$ and $3\sigma^{3\to 2} \simeq 0.969$ are satisfactorily close and mutually consistent.

To derive the lower bound, we first notice that the elementary tiles of Fig. 3, namely hexagons and rhombic dodecahedrons, perfectly tile the entire two- and three-dimensional space, respectively. In fact, it is possible to tile any d-dimensional Euclidean space with the shadow P of a unit cube of dimension $D = d+1$ projected along the $(1, 1, \ldots, 1)$ direction. To understand this, consider all the unit cubes of a D-dimensional hypercubic lattice the centers of which belong to the diagonal hyperplane of equation $\sum x_i = 0$. Their projection along the $(1, 1, \ldots, 1)$ direction is the desired tiling with the tile P. Now, such a polytope P can be tiled in two different ways with the D tiles of the $D \to D-1$ tilings under consideration, as shown in Fig. 3, and independently of its neighbors. If we have a total of N tiles, we have N/D such polytopes, which provides $2^{N/D}$ different tilings. Thus the total number of tilings is bounded below by $2^{N/D}$, which leads to the lower bound (70) on $\sigma^{D\to D-1}$.

To understand the upper bound, we begin with the $4 \to 3$ case. In 3-dimensional tilings, we extend the notion of de Bruijn lines and define de Bruijn surfaces. The latter are connected sets of rhombohedral tiles which share a common face orientation. In $4 \to 3$ tilings, there are four families F_i of such surfaces, since there are four possible edge orientations $\hat{\mathbf{e}}_i^{\parallel}$. In d-dimensional tilings, there are $(d-1)$-dimensional surfaces defined similarly. Like in the two-dimensional case, two adjacent surfaces of a same family cannot cross but can have contacts.

Like in Section 5.2, such a surface in a $4 \to 3$ tiling can be put in one-to-one correspondence with a $3 \to 2$ tiling, just as in a $3 \to 2$ tiling, a de Bruijn line can be seen as a directed random walk on a square grid like a $2 \to 1$ tiling. Therefore if we do not take contacts between surfaces

into account, a $4 \to 3$ tiling is a collection of independent $3 \to 2$ tilings, corresponding to all the de Bruijn surfaces of a given family. Of course, this approach will only provide an upper bound since contacts constraint the surfaces and reduce the entropy. Now the entropy of $3 \to 2$ tilings is known, and a fraction 3/4 of the tiles of the original $4 \to 3$ tilings belong to the de Bruijn surfaces of the family under consideration. Therefore

$$\sigma^{4\to 3} < \frac{3}{4}\sigma^{3\to 2} = 0.242. \tag{71}$$

Now, we can iterate the same argument in any dimension, thus getting that

$$\sigma^{D\to D-1} < \frac{D-1}{D}\sigma^{D-1\to D-2} < \frac{D-2}{D}\sigma^{D-2\to D-3} < \cdots < \frac{3}{D}\sigma^{3\to 2}, \tag{72}$$

which leads to the upper bound Eq. (70). The actual $4 \to 3$ entropy is strictly smaller than our bound (71), and its knowledge provides better upper bounds for larger D tilings. The best numerical estimate of this entropy is $\sigma^{4\to 3} = 0.214 \pm 0.002$,[48] which leads to $\sigma^{D\to D-1} < 4\sigma^{4\to 3}/D = (0.856 \pm 0.008)/D$ for $D \geqslant 4$, a noticeably better upper bound than (70). Similarly, the exact knowledge of any $D \to D-1$ entropy would provide a better upper bound for the entropy of tilings of dimension larger than D.

6. CONCLUSION

This paper studied random tiling models in the limit of high rotational symmetry. We developed a mean-field theory for tilings based on the iterative construction of rhombus tilings introduced by de Bruijn.[43] Our main goal is to improve on the knowledge of the tiling entropy. Table III summarizes the progress to-date. Evidently the mean-field theory is a considerable improvement upon earlier bounds.

The relevant quantity in our mean-field theory is the number of choices at each vertex, which is related to its coordination number (degree). In contrast to prior work that focused on the *mean* number of choices, the current study yields the *distribution* of the number of choices. Table IV demonstrates excellent agreement with numerical simulation.

We argue that high symmetry tilings become insensitive to phason strain, unlike finite symmetry tilings. In other words, phason elasticity vanishes at large codimension. In addition to the entropy and the phason elasticity, we considered finite size corrections and correlation functions.

Our mean-field theory does not take into account spatial correlations which should modify slightly the entropy. For example, if a vertex

has a low degree, it has less chance to be visited in the iterative process, which modifies the fixed point (36) and the entropy. Large degree vertices are more likely to be visited and to be split into two vertices of lower degree. We expect them to be less numerous than in our calculation (see Table IV), which accounts for the actual lower value of the entropy.

Our mean-field theory could be enhanced by inclusion of correlations. Instead of single vertices (with their arms and legs), one might instead study the statistics of pairs of vertices or even larger tiling patches and determine how these statistics evolve *via* the iterative process, when they are split into two pieces by a path going through them. It would also be useful to predict how the spatial correlations calculated in the paper perturb the mean-field entropy.

A second paper[36] follows this one and presents the numerical Monte Carlo study of large codimension tilings. In particular, it is demonstrated in this paper that in such tilings, the thermodynamic limit is restored: fixed boundaries do not result in the lowering of the entropy like in finite codimension cases.

APPENDIX A: CONSTRUCTION OF THE HEIGHT FUNCTION

This appendix constructs[42] the parallel and perpendicular spaces ($\mathcal{E}^{\parallel} = \boldsymbol{R}^2$ and $\mathcal{E}^{\perp} = \boldsymbol{R}^{D-2}$) for $D \to 2$ tilings as well as the mapping $h : \mathcal{E}^{\parallel} \to \mathcal{E}^{\perp}$. We embed these spaces in the D-dimensional hyperspace $\boldsymbol{R}^D$. Let the unit vectors $\{\hat{\mathbf{e}}_i\}$ be an orthonormal basis for $\boldsymbol{R}^D$. Their normalized projections into $\mathcal{E}^{\parallel}$ and $\mathcal{E}^{\perp}$ will be denoted, respectively, by $\hat{\mathbf{e}}_i^{\parallel}$ and $\hat{\mathbf{e}}_i^{\perp}$. Our first task is to represent these projections in the hyperspace basis.

We define the two-dimensional "parallel" space $\mathcal{E}^{\parallel}$ by its orthonormal basis

$$\begin{aligned} \hat{x}^{\parallel} &= \sqrt{\frac{2}{D}} \sum_{j=0}^{D-1} \hat{\mathbf{e}}_j \cos\left(\frac{\pi j}{D}\right), \\ \hat{y}^{\parallel} &= \sqrt{\frac{2}{D}} \sum_{j=0}^{D-1} \hat{\mathbf{e}}_j \sin\left(\frac{\pi j}{D}\right). \end{aligned} \tag{A.1}$$

Given the basis for $\mathcal{E}$ we define the projection operator $P_{\parallel}$ by $P_{\parallel}(u) \equiv (\hat{x}^{\parallel} \cdot u)\hat{x}^{\parallel} + (\hat{y}^{\parallel} \cdot u)\hat{y}^{\parallel}$ and its complement $P_{\perp} = 1 - P_{\parallel}$. The parallel space vectors $\hat{\mathbf{e}}_i^{\parallel}$ are the projections of suitably scaled hyperspace basis vectors,

$$\hat{\mathbf{e}}_i^{\parallel} \equiv P_{\parallel}(s_{\parallel}\hat{\mathbf{e}}_i). \tag{A.2}$$

Note that they form a regular fan

$$\hat{\mathbf{e}}_i^{\parallel} = \hat{x}^{\parallel} \cos\left(\frac{\pi i}{D}\right) + \hat{y}^{\parallel} \sin\left(\frac{\pi i}{D}\right). \tag{A.3}$$

By a "regular fan" we mean a collection of equally spaced vectors arranged in the upper half plane. The union of these vectors and their negatives forms a $2D$-fold symmetric star. We set the scale factor $s_{\parallel} = \sqrt{D/2}$ to normalize $\hat{\mathbf{e}}_i^{\parallel}$ in Eq. (A.3).

The $(D-2)$-dimensional "perpendicular" space $\mathcal{E}^{\perp}$ is the complement in $\boldsymbol{R}^D$ of $\mathcal{E}^{\parallel}$. Consider the projection of the scaled hyperspace vector $s_{\perp}\hat{\mathbf{e}}_i$ into $\mathcal{E}^{\perp}$, which we can express as

$$\hat{\mathbf{e}}_i^{\perp} \equiv P_{\perp}(s_{\perp}\hat{\mathbf{e}}_i) = s_{\perp}(\hat{\mathbf{e}}_i - P_{\parallel}\hat{\mathbf{e}}_i). \tag{A.4}$$

Its magnitude can be found from

$$\| P_{\perp} s_{\perp} \hat{\mathbf{e}}_i \|^2 = s_{\perp}^2 (1 + \| P_{\parallel} \hat{\mathbf{e}}_i \|^2 - 2\hat{\mathbf{e}}_i \cdot P_{\parallel} \hat{\mathbf{e}}_i) \equiv 1. \tag{A.5}$$

We evaluate $\| P_{\parallel} \hat{\mathbf{e}}_i \|^2 = 1/s_{\parallel}^2 = 2/D$ from Eq. (A.2), and we evaluate $\hat{\mathbf{e}}_i \cdot P_{\parallel}\hat{\mathbf{e}}_i = \sqrt{2/D}\hat{\mathbf{e}}_i \cdot \hat{\mathbf{e}}_i^{\parallel} = 2/D$ from Eq. (A.3) together with Eq. (A.1). Then Eq. (A.5) yields $s_{\perp} = 1/\sqrt{1-2/D}$. The following result will also be useful: if $i \neq j$ then

$$\hat{\mathbf{e}}_i^{\perp} \cdot \hat{\mathbf{e}}_j^{\perp} = -\frac{2}{D-2} \hat{\mathbf{e}}_i^{\parallel} \cdot \hat{\mathbf{e}}_j^{\parallel}. \tag{A.6}$$

Indeed, $\hat{\mathbf{e}}_i \cdot \hat{\mathbf{e}}_j = \delta_{ij} = \hat{\mathbf{e}}_i^{\parallel} \cdot \hat{\mathbf{e}}_j^{\parallel}/s_{\parallel}^2 + \hat{\mathbf{e}}_i^{\perp} \cdot \hat{\mathbf{e}}_j^{\perp}/s_{\perp}^2$.

Every vertex v in a rhombus tiling occupies a position of the form

$$\mathbf{r}_{\parallel}(v) = \sum_{i=1}^{D} \mathcal{R}_i(v) \hat{\mathbf{e}}_i^{\parallel} \in \mathcal{E}^{\parallel} \tag{A.7}$$

where the coefficients $\mathcal{R}_i$ are integers. To find the values of $\mathcal{R}_i$ for vertex v, choose any vertex as the origin for $\mathcal{E}^{\parallel}$, then follow a path of rhombus edges from the origin to v. Adding to (or subtracting from) $\mathcal{R}_i$ for each edge $\hat{\mathbf{e}}_i^{\parallel}$ along the path yields the values of $\mathcal{R}_i(v)$. The perpendicular space position of that vertex is defined as

$$h(\mathbf{r}_{\parallel}) = h(v) = \sum_{i=1}^{D} \mathcal{R}_i(v) \hat{\mathbf{e}}_i^{\perp} \in \mathcal{E}^{\perp}. \tag{A.8}$$

Values of $h(\mathbf{r})$ for $\mathbf{r}$ in the interior of a tile can be defined using linear interpolation on the values just defined for tile vertices.

The equation of a flat (strain-free) tiling, or of a locally flat tiling after coarse-graining is defined by D vectors $\boldsymbol{m}_i \in \mathcal{E}^{\parallel}$ such that

$$\mathcal{R}_i(v) = \boldsymbol{m}_i \cdot \mathbf{r}_{\parallel}, \tag{A.9}$$

the above equality meaning that $\mathcal{R}_i(v)$ is the closest integer to the right-hand side quantity. Then the $(D-2) \times 2$ phason gradient tensor $\boldsymbol{E} = \nabla_{\parallel} h(\mathbf{r}_{\parallel})$ is

$$\boldsymbol{E} = \sum_{i=1}^{D} \hat{\mathbf{e}}_i^{\perp} \otimes \boldsymbol{m}_i, \tag{A.10}$$

where $\hat{\mathbf{e}}_i^{\perp} \otimes \boldsymbol{m}_i$ is a the tensor product of the *column* vector $\hat{\mathbf{e}}_i^{\perp}$ and the *line* vector $\boldsymbol{m}_i$.

ACKNOWLEDGMENTS

We thank Chris Henley and Pavel Kalugin for useful discussions. This research is supported in part by the National Science Foundation under grants DMR-0111198 and INT-9603372 and by the CNRS.

REFERENCES

1. D. Shechtman, *et al.*, *Phys. Rev. Lett.* **53**:1951 (1984).
2. D. Levine and P. J. Steinhardt, *Phys. Rev. Lett.* **53**:2477 (1984).
3. R. Penrose, *Bull. Inst. Math. Appl.* **10**:226 (1974).
4. V. Elser, *Phys. Rev. Lett.* **54**:1730 (1985).
5. C. L. Henley, *in* D. P. Di Vincenzo and P. J. Steinhart eds. *Quasicrystals, the State of the Art* (World Scientific, 1991), p. 429.
6. M. Widom, K. J. Strandburg, and R. H. Swendsen, *Phys. Rev. Lett.* **58**:706 (1987).
7. F. Lançon, L. Billard and P. Chaudhari, *Europhys. Lett.* **2**:625 (1986).
8. H.-C. Jeong and P. J. Steinhardt, *Phys. Rev. Lett.* **73**:1943 (1994); K. Ingersent and P. J. Steinhardt, *Phys. Rev. Lett.*, **64**:2034 (1990).
9. M. Widom, in M.V. Jaric and S. Lundqvist eds. *Quasicrystals* (World Scientific, 1990), p. 337.
10. R. Mosseri and F. Bailly, *Int. J. Mod. Phys. B* **6&7**:1427 (1993).
11. N. Destainville, R. Mosseri, and F. Bailly, *J. Stat. Phys.* **87**:697 (1997).
12. N. Destainville, R. Mosseri, and F. Bailly, *J. Stat. Phys.* **102**:147 (2001).
13. A. Björner, M. Las Vergnas, B. Sturmfels, N. White, and G. M. Ziegler *Oriented Matroids*, (Cambridge University Press, 1993).
14. R. Kenyon, *Algorithmica* **9**:382 (1993).
15. S. Elnitsky, *J. Combinatorial Theory A* **77**:193–221 (1997).

16. G. D. Bailey, *Tilings of Zonotopes: Discriminental Arrangements, Oriented Matroids, and Enumeration*, Ph. D. Thesis (University of Minnesota, 1997).
17. H. Cohn, M. Larsen, and J. Propp, *New York J. of Math.* **4**:137 (1998).
18. H. Cohn, R. Kenyon, and J. Propp, *J. of the AMS* **14**:297 (2001).
19. R. Cerf and R. Kenyon, *Comm. Math. Phys.* **222**:147 (2001).
20. M. Latapy, *RAIRO-Theor. Inf. Appl.* **36**:389 (2002).
21. H. W. J. Blöte and H.J. Hilhorst, *J. Phys. A: Math. Gen.* **15**:L631 (1982).
22. M. Widom *Phys. Rev. Lett.* **70**:2094 (1993); P. Kalugin *J. Phys. A: Math. Gen.* **27**:3599 (1994); J. de Gier, B. Nienhuis, *Phys. Rev. Lett.* **76**:2918 (1996); J. de Gier and B. Nienhuis, *J. Phys. A: Math. Gen.* **31**:2141 (1998).
23. B. Nienhuis, *Phys. Rep.* **301**:271 (1998).
24. D. M. Knuth, Axioms and Hulls, *Lect. Notes in Computer Sci.* **606**:35 (1992).
25. M. Widom, N. Destainville, R. Mosseri, and F. Bailly, *in Proceedings of the 6th International Conference on Quasicrystals*, (World Scientific, Singapore, 1997).
26. M. V. Jaric and S. L. Johnson, *Phys. Lett. A* **219**:238 (1996); C. Zeng, J. Kondev, D. McNamara and A.A. Middleton, *Phys. Rev. Lett.* **80**:109 (1998).
27. K. J. Strandburg, L.-H. Tang and M. V. Jaric *Phys. Rev. Lett.* **63**:314 (1989); L. J. Shaw, V. Elser, and C. L. Henley, *Phys. Rev. B* **43**:3423 (1989); L.-H. Tang, *Phys. Rev. Lett.* **64**:2390 (1990); M. Oxborrow and C. L. Henley, *Phys. Rev. B* **48**:6966 (1993); F. Gahler, Proc. ICQ5 236 (1995); D. Joseph and M. Baake, *J. Phys. A* **29**:6709 (1996).
28. M. Widom, D. P. Deng and C. L. Henley, *Phys. Rev. Lett.* **63**:310 (1989); L. J. Shaw and C. L. Henley, *J. Phys. A* **24**:4129 (1991); M.E.J. Newman and C.L. Henley, *Phys. Rev. B* **52**:6386 (1995).
29. C. Itzykson, J.-M. Drouffe, *Statistical Field Theory*, Vol. 1 (Cambridge Monographs on Mathematical Physics, 1992).
30. V. E. Korepin, F. Gahler and J. Rhyner, *Acta Cryst. A* **44**:667 (1988).
31. J. E. S. Socolar, P.J. Steinhardt and D. Levine, *Phys. Rev. B* **32**:5547 (1985).
32. D. A. Rabson, N. D. Mermin, D. S. Rokhsar and D. C. Wright, *Rev. Mod. Phys.* **63**:699 (1991).
33. B. Bollobas *Random graphs* (Academic Press, New York, 1985).
34. J. Vidal, N. Destainville, and R. Mosseri, *Phys. Rev. B* **68**:172202 (2003).
35. N. Destainville, M. Widom, R. Mosseri, and F. Bailly, *Mat. Sci. Eng. A* **294**:409 (2000).
36. M. Widom, N. Destainville, R. Mosseri, and F. Bailly, Random tilings with high symmetry: II. Boundary conditions and numerical studies, *J. Stat. Phys.* **120**(5/6):837–873 (2005).
37. V. Elser, *J. Phys. A* **17**:1509 (1984).
38. G. H. Wannier, *Phys. Rev.* **79**:357 (1950); *Phys. Rev.* B **7**:5017 (E 1973).
39. N. Destainville, *J. Phys. A: Math. Gen* **31**:6123 (1998).
40. H. S. M. Coxeter, *Regular Polytopes* (Dover, 1973).
41. V. Desoutter, N. Destainville, *J. Phys. A: Math. Gen.* **38**:17 (2005).
42. W. Li, H. Park, and M. Widom, *J. Stat. Phys.* **66**:1 (1992).
43. N. G. de Bruijn, *Ned. Akad. Wetensch. Proc. A* **84**:39 (1981); *J. Phys. France* **47**:C3–9 (1986).
44. J. E. S. Socolar, P. J. Steinhardt and D. Levine, *Phys. Rev. B* **32**(8):5547 (1985).
45. F. Gähler and J. Rhyner, *J. Phys. A: Math. Gen.* **19**:267 (1986).
46. C. L. Henley, *J. Phys. A: Math. Gen.* **21**:1649 (1988).
47. M. E. Fisher, *J. Stat. Phys.* **34**:667 (1984).
48. M. Widom, R. Mosseri, N. Destainville, F. Bailly, *J. Stat. Phys.* **109**:945 (2002).
49. K. J. Standburg, *Phys. Rev. B* **44**:4644 (1991).